NOVEL INTERNAL SENSORS FOR HELICOPTER MAIN ROTOR GEARBOXES

Dr Matthew Greaves
Head, Safety and Accident Investigation Centre
Cranfield University
Cranfield, Beds. MK43 0AL
United Kingdom

Dr Lionel Tauszig
Project Certification Manager, Rotorcraft
European Aviation Safety Agency
Ottoplatz 1, 50679 Cologne
Germany

Faris Elasha
Research Fellow
Cranfield University
Cranfield, Beds. MK43 0AL
United Kingdom

Prof David Mba
School of Engineering
London South Bank University
90 London Road, London SE1 6LN
United Kingdom

Abstract

Since the 1980s, the use of onboard sensors for helicopter health and usage monitoring systems (HUMS) has been increasingly popular for benefits of enhanced safety. However, despite these successes, recent accidents, such as that to G-REDL, have raised questions about the efficacy and limitations of HUMS systems. This paper presents an overview of an EASA-funded project looking into the use of internal sensors in helicopter main rotor gearboxes for the improved detection of incipient damage. It details the process of: reviewing the failure modes; selecting a sensing technology; lab-scale testing of the sensor and wireless transmission; and implementation and successful full-scale testing of a prototype system.

1. INTRODUCTION

This paper describes work undertaken as part of EASA project '*EASA.2012.OP.13 VHM*'. This is the first publication from the project, and as such will outline the project phases, the work undertaken and some of the setbacks and achievements.

The project was initiated in response to two recommendations from the UK Air Accidents Investigation Branch (AAIB), namely:

> *UNKG-2011-041: It is recommended that the European Aviation Safety Agency research methods for improving the detection of component degradation in helicopter epicyclic planet gear bearings.*
>
> *UNKG-2010-027: It is recommended that the European Aviation Safety Agency, with the assistance of the Civil Aviation Authority, conduct a review of options for extending the scope of Health and Usage monitoring Systems (HUMS) detection into the rotating systems of helicopters.*

2. BACKGROUND TO THE PROJECT

Since the 1980s, the use of onboard sensors for helicopter health and usage monitoring systems (HUMS) has been increasingly popular for benefits of enhanced safety. Through the years, a wide range of sensors and methodologies have been developed for monitoring and fault detection across helicopter rotor, drivetrain and engine systems. Vibration Health Monitoring equipment is now commonplace on large helicopters and the technology has matured and can claim a number of successes with respect to accident prevention.

However, despite these successes, recent accidents, such as that to G-REDL[1], have raised questions about the efficacy and limitations of HUMS systems. Therefore, it is appropriate that the issue of detecting incipient failure is re-examined, particularly in light of technological advances since the development of the early HUMS systems.

The research programme described here aims to inform the next generation of HUMS systems by identifying and proving feasibility for new, and newly-applied, sensing technologies, with a specific focus on internal sensors.

2.1. Overview of VHM Systems

HUMS was developed in North Sea operations, motivated in part by the crash to a Boeing Vertol 234 in 1986 which was caused by disintegration of the forward main gearbox. After development in the 1990s, the UK CAA mandated fitment of HUMS to certain helicopters. One article suggests that HUMS "successes" are found at a frequency of 22 per 100,000 flight hours[2].

Several surveys have been carried out by different authors and agencies into the effectiveness of HUMS sensors and analysis methods. The FAA carried out one of the first surveys for helicopter HUMS[3] in an effort to develop certification requirements. NASA performed several surveys[4-7] examining the application of HUMS in areas ranging from gearbox to engine health monitoring. The UK CAA has also conducted a review of extending HUMS to rotor systems[8]. Those surveys provide a good overview of existing sensor technology and methods and their implementation in a HUMS programme.

2.2. Signal Processing

There is an extensive range of possible signal processing techniques available with which to analyse HUMS vibration signals. Over the years, processing has evolved from simple indicators such as RMS to more developed techniques such as data mining[9-22]. One more recent development is the implementation of an Advanced Anomaly Detection algorithm, developed by GE under a UK CAA sponsored programme[23]. This expands the concept of condition indicators to establish a "normal" vibration set which allows alerts to be raised using a data mining approach.

The main aim of any signal processing technique is to 'expose' the signal which characterises the degradation or incipient failure, from the general noise of the platform and ordinary gear meshing and bearing noise. However, the ultimate success of any signal processing strategy depends on the quality of the signal under analysis; if the signal-to-noise ratio is too small then no amount of processing will allow detection.

The initial aim of this research project was to focus on the sensing technologies available for fault detection, with a particular emphasis on increasing the signal-to-noise ratio of the 'defect signal' measured against the background noise level, rather than on improved processing of existing signals. However, as the project progressed, both aspects were explored.

3. ACCIDENT REVIEW AND FAILURE MODES

A review of accidents and failure modes was conducted in order to understand the types of failures which cause catastrophic failures and to help select case studies for benchmarking candidate technologies.

The fundamental generic degradation and failure mechanisms for gears and bearings are well understood and include effects such as: wear, spalling, adhesion, fretting etc.

Roberts, Stone and Turner[24] analysed over 1,000 accident reports for the Bell 206. They discovered 29 accidents involving engine and powertrain failures, involving 10 different failure types. These were listed as: bond failure; corrosion; fatigue; fracture; fretting; galling and seizure; human; stress rupture; thermal shock and wear.

For this project, a thorough search was conducted, via various available databases and data sources, to form a comprehensive population of relevant helicopter accident and incident formal reports. Candidate accident reports were selected according to strict specified criteria:

i. Final official formal reports.
ii. Of sufficient technical detail so as to establish an adequate sequence of events.
iii. Either of events within the MGB and Transmission systems, or of external events that influence these systems (including human input).
iv. Of relevance to existence and application of Health and Usability Monitoring Systems.
v. Written in English (there was no access to the whole group of Eastern helicopters for instance, or to Western reports written in other languages due to time limitations).

Applying the above criteria, a total of 12 reports were selected out of an initial screening input of 413. The selected accidents can be summarised by registration as:

G-REDW/CHCN	C-FHHD	G-REDL
G-BJVX	C-GZCH	G-BBHM
G-CHCF	G-ASNL	G-PUMI
9M-SSC	G-JSAR	LN-OPG.

In order to support the selection, the European Helicopter Safety Analysis Team (EHSAT) database was interrogated using different criteria, aiming to capture any significant accidents that had been missed. However, no new accidents were discovered thereby providing some confidence that the earlier sort process had not missed any significant accidents*.

Detailed fault tree analysis was performed to identify various primary and secondary failures of the MGB and Transmission systems for each of the selected cases. The fundamental aim of the fault tree analysis was to develop detailed understanding of triggers, causes, and event sequences for these accidents and incidents.

The analysis showed that there is no general pattern or sequence to these accidents. There may be some similarities in some events, but the overall sequence, nature, depth, or importance of each event is found to be different either up or down stream of the accident.

The key failure modes identified from the above analysis were:

- Small corrosion pits as triggers of cracks.
- Small machining defects as triggers of cracks.
- Sub-surface cracks
- Possible spalling of gears/ bearings
- Material defects/ manufacturing anomalies
- Galling of studs/ bolts
- Wear due to variations loads/ movements
- Fracture/ rupture under overload.
- Deformation under overload of bearing rollers/ raceways/ gear teeth/ shafts/ splines

* The investigations into B-MHJ and B-HRN were on-going and hence were not included in the analysis

- Internal residual hoop/ tension/ torsion/ compression/ buckling stresses.
- Permanent distortion (creep) of casings
- Seizure of roller bearing
- Improper coating of hardmetal (carbide grains size, porosity, coating thickness, etc)
- Lamination of the hard metal coating.
- Defective bonding between hard metal and coating

Given how different each of the accidents examined is, there was an argument to be made for using all of the accidents as test cases. However, given the time and funding available this was not practical. It also risked diluting the focus of the research.

Instead, it was decided to place the focus on the monitoring of planetary gears and bearings as motivated by the recommendation stemming from the accident to G-REDL (*UNKG-2011-041)*. This is considered to be the most complex case, and hence any monitoring solution that can be effectively applied to this scenario stands a good chance of being successful in monitoring, say, bevel gear shafts or possibly transferring to other rotating systems on the aircraft.

4. SENSING TECHNOLOGY REVIEW AND SELECTION

In order to review the potential sensing technologies, all options were initially considered. Opinions and technologies were sought from a range of subject areas, including: wind turbines; motorsport; rail; and marine. Whilst some innovative practices were discovered, no entirely new technologies were discovered.

A down-selection process was then undertaken, leaving: vibration; strain; temperature; acoustic emission; and audible acoustics as potential sensing technologies.

4.1. Operating conditions

Clearly any solution will need to function correctly in an operational environment. Therefore, it was necessary to establish baseline operating requirements for any proposed sensor. Precise conditions differ on each platform and so in general a 'worst case' assessment was used.

A number of constraints were imposed to limit the possible solution:

- No mechanical signal connection (e.g. slip rings) - wireless only
- Limited space (of the order of cm at most)
- Useful temperature range -10˚C to +130˚C
- Sensor weight below 10g
- Tolerant of gearbox mineral oil
- Power inside MGB is generated – no battery
- Guaranteed attachment, or no risk from sensor if detached

Based on these requirements it was decided to pursue acoustic emission (AE) as the sensing technology. AE measurement is the capture of high frequency (hundreds of kilohertz) surface stress waves that are produced in structures by applied forces. The potential of this technology has increased dramatically over the last 10 years due to improvements in sensor and data acquisition technology such that it is now established as a condition monitoring tool.

5. WIRELESS TRANSMISSION

Having selected a potential sensing technology, it was necessary to ensure that a suitable wireless transmission technique could be found or developed to complement it that could operate successfully inside the gearbox.

5.1. Existing Systems

There are a range of established technologies which might provide a starting point for such a system, including Wifi, Bluetooth and ZigBee. Table 1 details some of the key parameters of these three protocols.

	WiFi	Bluetooth	ZigBee
Standard	IEEE 802.11	IEEE 802.15	IEEE 802.15
Max range	50-100m	10-100m	10-100m
Frequency	2.4 and 2.5 GHz	2.4 GHz	868 MHz Europe 900 - 928 MHz US 2.4 GHz World
Power consumption	High	Medium	Low
Max network speed	>11 Mbps	700 kbps – 1 Mbps	20 kbps - 250 kbps
Network join time		3 s	30 ms

Table 1. Candidate wireless communication protocols

One key feature of Acoustic Emission is the frequency range of interest e.g. around 100 kHz to 1 MHz. Therefore, to produce an unaliased signal at 16 bit resolution would require a data rate of 32 Mbps.

ZigBee offers low power consumption and short join time which are useful in this application, but it also has a limited network speed which will not handle sampling rates in the order of MHz (ZigBee can support around 16 kHz sampling rates at 16 bit resolution). Bluetooth can offer higher transmission rates and hence support higher sampling rates (64

kHz at 16 bit resolution) although this will still not permit real-time MHz sampling rates. A 2 MHz sampling rate at 32 bit resolution would require sustained 32 Mbps which would be challenging for even WiFi standards. Therefore, any of these wireless protocols will require pre-processing or caching to work at high acoustic emission sampling rates. However, typical vibration sampling rates can be easily supported.

There is an additional factor of shielding which greatly complicates the use of wireless transmission. The MGB casing acts as a Faraday Cage, defeating attempts to pass an electromagnetic wave through the casing. This means that placing an antenna outside the gearbox will not allow a signal to be transmitted into the gearbox. There will also be shielding and modulating effects from the rotating metallic components inside the gearbox, meaning that any Transverse Electromagnetic (TEM) field may be affected or defeated inside the gearbox. Within an enclosed metal cavity, the use of high frequencies produces a standing wave pattern, where the field falls to zero at regular intervals, typically every half wavelength (about 6 cm at 2.4 GHz). If the receive coil passes through these standing wave nulls, the recovered power will vary, and unwanted modulation will be superimposed on the recovered baseband signal.

Alignment in the gearbox also introduces complexity. Using a high gain antenna would produce a spot beam where the power density is very high, so the rotating part must remain in the spot at all times. Additionally, unless circular polarisation is used on both transmit and receive antennas, the recovered power will vary at the rotation rate.

A further consideration is the availability of power; it would be preferable if power were transferred wirelessly along with the data. RF scavenging to supply dc power wirelessly in tags, has been carried out at the relatively high RF frequencies of 800 MHz and 2.4 GHz. Using an antenna with high gain allows useful power to be transmitted over a long range, in the order of many tens of meters, using a few Watts of RF. Note that these systems are termed “far field” and energy transfer is by TEM wave. Huang[25] has demonstrated the transfer of AE signals and power using far field waves at 2.4 GHz.

A final consideration is the generation of sufficient RF power and licensing. For these reasons it was decided to use the 13.56 MHz ISM band, used by other near field, short range devices, such as ISO14443 contactless cards e.g. Mastercard PAYPASS and TFL Oyster cards.

5.2.Newly developed system

In an attempt to meet the demands outlined in the previous section, a new approach was developed to wireless transmission of AE signals.

The system uses a a so-called “homodyne” (same–frequency) receiver with a “modulated backscatter” communications link, to pass the analogue signal across the wireless link. Operation at 13.56 MHz allows the use of magnetic coupling, where the “antennas” are two tuned loops of wire or pipe. Such coupling is termed “near field” and relies purely on magnetic coupling, as seen in a conventional transformer for AC mains. The magnetic loop does not produce a TEM “propagating” wave, as in a normal broadcast transmitter. By using two parallel, coaxial coils in close proximity, the coupling remains consistent as one coil rotates with respect to the other.

5.3.Method of operation

“Modulated backscatter” is a technique that relies on periodic damping of the resonant circuit of the rotating loop. When magnetically coupled to a receiving loop, the modulation may be detected. In contactless cards, the data is transmitted digitally by modulating a carrier signal with a square wave. However, in this application, there is a need to transmit a linear analogue signal over a bandwidth extending from 100 kHz to 1 MHz, to preserve the shape of the sensor time domain waveform.

Contactless cards use a “load” modulation scheme, where a damping resistor is switched periodically in parallel with the coil. This is accomplished with a simple on/off FET switch, but the technique is not suitable for a linear system.

As previously discussed, digital transmission of sensor data up to 1 MHz bandwidth would occupy too much bandwidth for a back-scatter technique and would make the sensor circuitry quite complex.

A better analogue modulation scheme is to modulate the resonant frequency of the loop using a varactor diode. Such a diode is a variable capacitor controlled by a “tuning” voltage and has a linear response over a certain voltage range. The electrical change so induced by the varactor diode produces a combination of amplitude and phase modulation of the back-scattered signal.

The back-scattered signal can be “tapped off” the illuminating coil, so a single coil functions both as transmitter and receiver simultaneously. Using a high quality (low noise) crystal oscillator as both transmit source and receiver reference, enables the use of homodyne receiver architecture. A portion of the transmitted signal (which is free of modulation) is multiplied with the backscattered signal from the tap at the same carrier frequency, in a coherent demodulator. The output of the demodulator, which responds to both amplitude and phase modulation, is filtered to remove the RF at 13.56 MHz leaving the baseband signal.

6. LAB-SCALE SENSOR TEST

In order to understand, test and validate the performance of acoustic emission as a sensing technique, a range of lab-scale tests were performed. By seeding faults in a representative setup it was possible to identify the detection potential of AE, for a range of faults, in a controlled condition, particularly in comparison with more established vibration techniques. To provide the most representative test conditions with which to study a helicopter gearbox, an existing rig was heavily modified as shown in Figure 1.

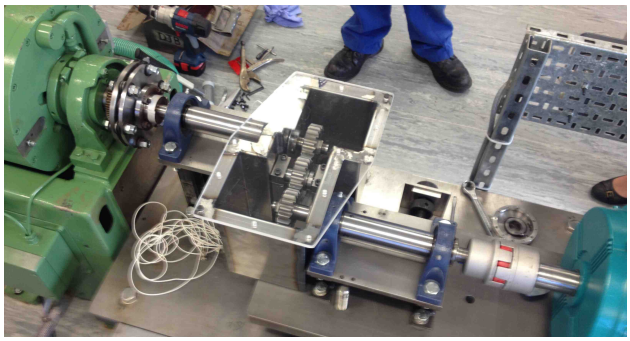


Figure 1.Lab-scale gear rig

The rig uses three gears, an input gear, an idler gear and an output gear, to approximate a single planet of an epicyclic setup. The input gear is driven by a fixed speed motor, and the output gear is loaded by a variable dynamometer. The idler gear was allowed to rotate about a fixed idler shaft by two taper roller bearings.

A miniature triaxial accelerometer was mounted on the idler shaft next to a miniature AE sensor as shown in Figure 2.

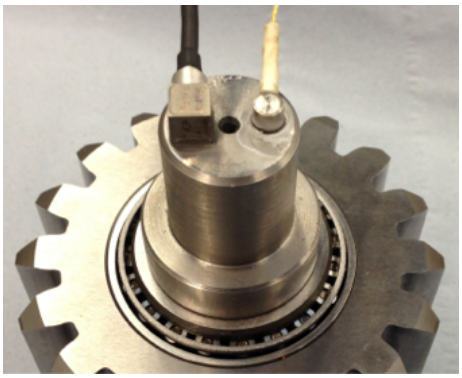


Figure 2. Triaxial accelerometer and AE sensor mounted on idler shaft

Three levels of damage were introduced to one of the bearings using electro-discharge machining (EDM): gross (a 2 mm wide, 1 mm deep slot in the outer race); marginal (2 mm diameter spot, 0.5 mm deep); and slight (1 mm diameter spot, 0.25 mm deep) – see Figure 3.

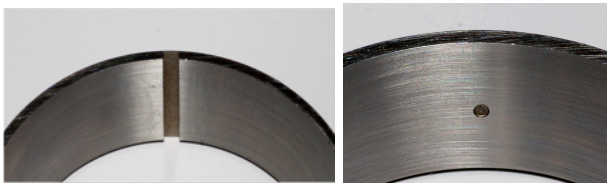


Figure 3. Gross and slight bearing outer race damage

6.1.Enhanced Signal Processing

Whilst the gross damage was easily detected using traditional techniques, the more subtle damage was much more difficult to detect. The use of taper roller bearings may have limited the detectability because of the ability of the roller to bridge the 'hole'. In addition, the use of EDM may have removed the rough edges, often seen in damage, which can help to provide AE events. As a result, enhanced signal processing was used to try and extract useful information.

Signal separation techniques have been applied in the diagnosis of bearing faults within gearboxes in more recent times. The separation is based on decomposing the signal into deterministic and random components. The deterministic part represents the gear component and the random part represents the bearing component of the measured signal. The bearing contribution to the signal is expected to be random due to slip effects[26-29].

A number of methods for signal separation are available, each having relative advantages and disadvantages[27,30-32]. Techniques such as Linear Prediction (LP) have been employed for separation, however, LP is applied only to stationary vibration signatures. To overcome the problem of separation of non-stationary vibrations, adaptive filters were proposed. This concept is based on the Wold Theorem, in which the signal can be decomposed into deterministic and non-deterministic parts. The separation is based on the fact that the deterministic part has a longer correlation than the random part and therefore the autocorrelation is used to distinguish the deterministic part from the random part. A reference signal is required to perform the separation, however, for practical diagnostics, the reference signal is not always readily available. As an alternative, a delayed version of the signal has been proposed as a reference signal and this method is known as self-adaptive noise cancellation (SANC)[29] which is based on delaying the signal until the noise correlation is diminished and only the deterministic part is correlated.

The Spectral Kurtosis technique has been introduced recently for bearing signal separation[33-35]. The basic principle of this method is to determine the Kurtosis at different frequency bands in order to identify the energy distribution of the signal and determine where the high impact energy (transient

events) are located in the frequency domain. It has been demonstrated to be effective even in the presence of strong additive noise[35].

The Spectral Kurtosis was employed to extract the filter characteristics which were utilised for envelope analysis on the non-deterministic component of the AE signature. A comparison of the vibration and AE analysis showed both measurements were able to identify the presence of the large bearing defect based on observations in the enveloped spectra. For the small defect condition however, the enveloped spectrum was dominated by the gear mesh frequencies and their harmonics, and as such the bearing defect frequencies were not evident in the vibration signal. However AE analysis was able to identify both the small and large defect conditions. Detection of the small bearing defect gives the AE measurement a diagnosis advantage over the vibration signal. The Figures overleaf show the separated signal, SK and the enveloped spectrum with the outer race defect (ORD) frequency shown.

7. LAB-SCALE WIRELESS SYSTEM

In order to test the approach described in Section 5, a prototype system was constructed. This consisted of two coils (to replicate a fixed and rotating coil) with one attached to a sensor conditioning board, which accepts a signal input, and the other attached to a demodulator producing an output signal.

A high stability oscillator is used as the transmit source and to ensure the oscillator is not adversely loaded, a buffer amplifier is used to drive a power amplifier producing approximately 1 Watt of RF output into the illuminator coil. The buffer amplifier is also required to ensure that the carrier signal has no backscatter modulation present on it, as a pure sine wave carrier is needed as a reference in the coherent demodulator.

7.1. Coherent demodulator and filter

The receive input from the illuminator coil tap is fed to a demodulator IC. The baseband output from the demodulator is buffered and fed to a low pass filter to drive a final amplifier. The carrier input to the demodulator is obtained by a connection to the crystal oscillator, through a phase shift network. The carrier phase shifter is necessary to correctly align the carrier phase with the backscattered phase, to obtain the highest baseband output possible from the demodulator IC.

7.2. Rotating coil and sensor

The receive loop is tuned by a capacitor to bring it to resonance just above 13.56 MHz. A rectifier produces a dc voltage, which is smoothed for an opamp. The opamp has a gain bandwidth product of 18 MHz and draws 3 mA from a 3.6 V supply.

The sensor output is fed into the high impedance input of the opamp to avoid loading the sensor output. The output feeds a low pass trap to ensure the very high levels of 13.56 MHz do not appear at the amplifier's output pin, but pass the 1 MHz sensor signal to the varactor diode. A small dc voltage is provided to bias the varactor into its most linear region. With no sensor signal applied to the varactor (just the bias voltage), its capacitance brings the resonance of the circuit to precisely 13.56 MHz

7.3. Transmit loop (fixed part)

To set the coil's quality factor (Q), a resistor is used which also allows a tap-off for the backscattered field. The Q factor has to be adjusted to allow sufficient Q for the transmission of power, but not too high to limit the system bandwidth, which would cause a drop off in the response at 1 MHz.

7.4. Set up and test of the system

After installation the system needs to be tuned as the spacing between the coils changes their mutual coupling, Q and bandwidth and this alters the values needed on the matching network. By tuning components on the fixed coil circuitry, the flattest response, at the expense of signal amplitude can be achieved.

When installing the sensor board against a metal object, it was necessary to use ARC WAVE-X to avoid detuning the coils. This is a flexible EMI/RF absorber, which allows the coils to be close to metal without being detuned.

Investigating the frequency behavior of the lab-scale system, the system behaves in a broadly linear way in the 100 kHz to 1 MHz range.

The only known shortcoming of the lab-scale system is the effect of dispersion on the sensor signal, which will be displayed in the time domain. Dispersion, sometimes known as non-linear group delay, results when different frequency components in the baseband signal are delayed by different times as they pass through the circuitry. The main cause of dispersion is the sharp phase response of the tuned resonator consisting of the two coils and their mutual coupling. The high Q (and thus dispersive response) is needed to transfer power efficiently, otherwise much of the RF power would be wasted in the series resistor at the base of the coil.

If the dispersion is consistent, then it can be corrected using software, by delaying different frequencies by appropriate amounts and then reconstructing the time signal.

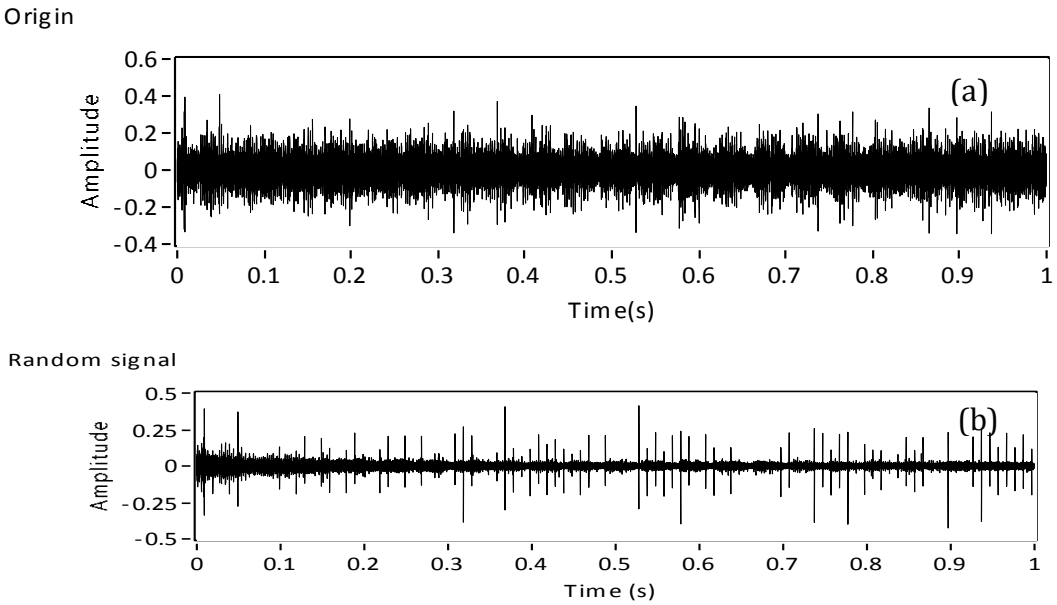


Figure 4.Time waveform of AE signal (a) before and (b) after separation

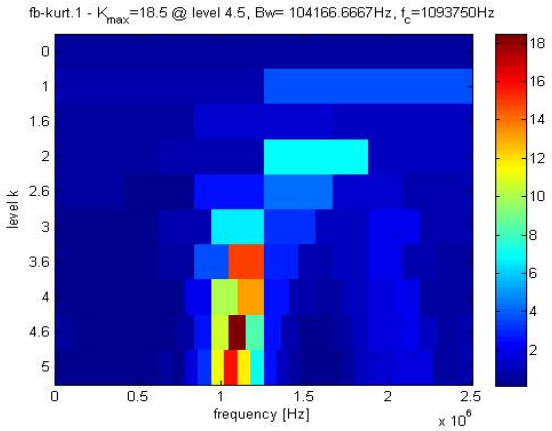


Figure 5. SK kurtograms for small bearing defects

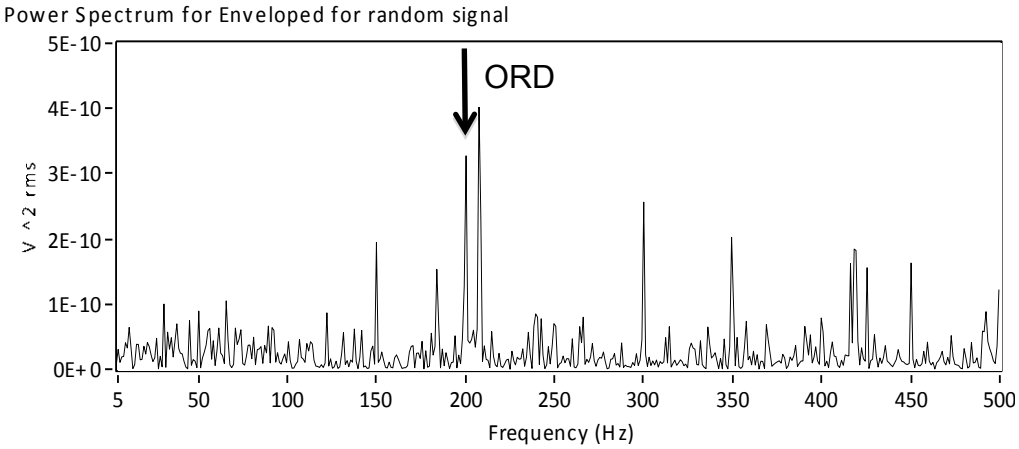


Figure 6. Enveloped spectrum of AE signal with small bearing defects

8. FULL-SCALE TESTING

In order to test and validate the approach outlined by the lab-scale testing, it was necessary to perform full-scale testing of the acoustic emission and wireless transmission concept. Whilst the lab-scale approach tentatively proved the concept, many of the issues surrounding new techniques are only revealed when it is implemented at full-scale.

For this phase of testing, an SA 330 Puma gearbox was acquired. Whilst this gearbox is an older design, it was the basis of the design of the current EC225 main gearbox, and shares many of the same design features. Most importantly for this project, it has a final two-stage epicyclic reduction utilizing a combined planet gear / outer bearing race design. Airbus Helicopters provided technical support and access to their test bench facilities and testing was conducted in May / June of 2014 (see Figure 11).

8.1.AE sensor selection

Having selected AE as the detection mechanism, it was necessary to select a sensor for use inside the MGB and Figure 7 shows the range chosen for the project. All of the sensors considered required signal conditioning and/or pre-amplification. Research by Pickwel[36] showed that the development of a functioning micro AE sensor (approximately 20 µm thick) was possible and comparison with commercial AE sensors provided some confidence in the performance of the sensor. However, this research work focused more on the design and physical production of these sensors rather than the detail of their performance.

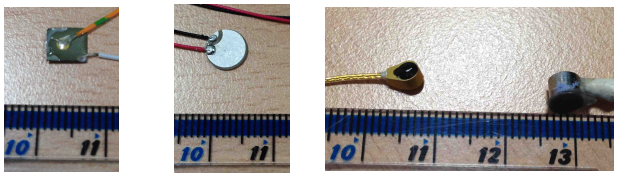


Figure 7. Potential AE sensors (L-R) micro, PWAS, s9225 and Pico

The piezoelectric-wafer active sensor (PWAS) is a small sensor often used for NDE testing and condition monitoring[37]. A 7 mm diameter, 0.2 mm thick sensor was selected for comparison.

The s9225 sensor is a miniature (3.6 mm x 2.4 mm) acoustic emission sensor from Physical Acoustics weighing less than 1 gram, with an operating range from 300 kHz upwards.

The Physical Acoustics Pico sensor, is a miniature (5 mm diameter, 4 mm height) acoustic emission sensor weighing less than 1 gram. This was the sensor used in the lab-scale testing.

There was a need to balance reliability and stability against the potential damage if released. The Pico is a reliable COTS sensor, but would cause significant damage if released into a planet bearing. The micro sensor is the smallest of the sensors but is experimental and susceptible to noise. Therefore, a comparison between the PWAS and s9225 sensors was conducted on the lab-scale rig, with the PWAS proving more effective. This sensor was used for the full-scale test programme. An additional feature of the PWAS sensor is its very broadband performance (from low kilohertz up to Megahertz). This means that it is able to function to detect more traditional vibration frequency ranges as well as AE ranges.

8.2.Experimental setup

A test programme was devised consisting of tests in three conditions – an undamaged planet bearing; a heavily damaged planet bearing; and a slightly damaged planet bearing. The different conditions were achieved by swapping a planet gear between each test. Each of these three conditions was tested at a range of loads.

The damage geometry was approximated as a rectangle with fixed depth and width. The fault-to-rolling element length ratio dictates whether the fault is extended (major) or not (minor). The defect length for the major damage was 30 mm and 10 mm for the minor damage and around 0.3mm deep for both cases.

In its current form, the wireless transfer system is only able to support a single sensor, and therefore it was necessary to select a location at which to attach the sensor. One of the restrictions to the positioning of the sensor was the need to keep the sensor clear of the main upper face of the planet carrier to allow it to be used as pressure face when changing the planet gears. The sensor was bonded in a position on the 'dish' of the planet carrier, as shown in Figure 8 and Figure 9 below.

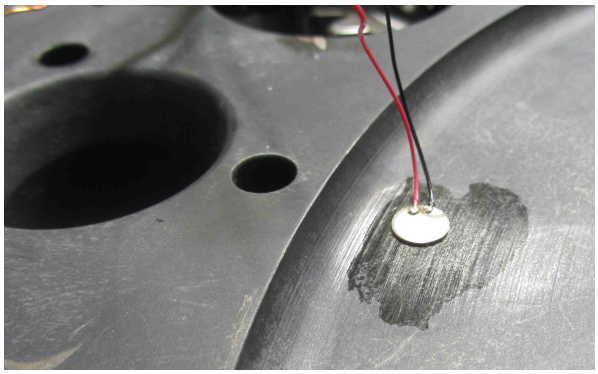


Figure 8. Sensor position on dish of planet carrier

For the full-scale wireless system, the prototype system was modified and rebuilt for operation inside the Puma gearbox. Whilst the principles and transfer mechanisms of the lab-scale design remained the same, there were changes to most aspects of the system.

One of the most significant changes from the lab-scale system was that the space available to mount coaxial coils on the planet carrier and the gearbox casing is limited. The full-scale system comprised two single turn brass coils of approximately 400 mm diameter which were cut to size using water jets for accuracy. The stationary (upper) coil was suspended from two clamping rings which were attached to the top case of the gearbox with a spacer through the holes to retain location. The moving (lower) coil was attached to a circular mounting ring which was in turn mounted on top of the oil caps on the planet carrier (see Figure 9).

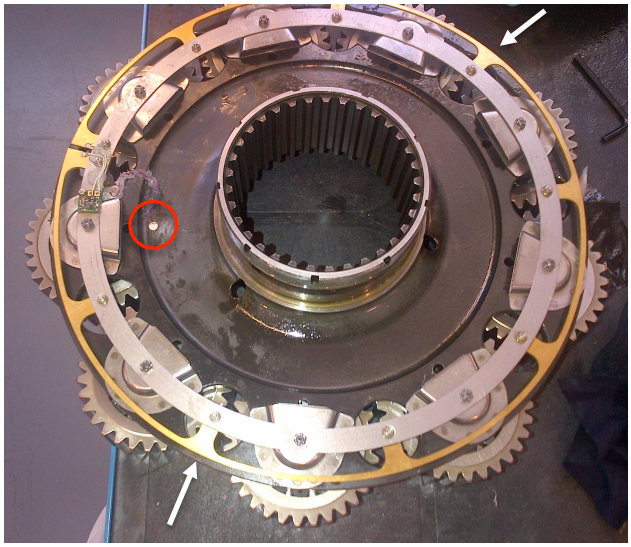


Figure 9. Moving coil mounted on the planetary carrier (coil arrowed, sensor circled)

Figure 10 shows the two coils in position before the top cover was pressed onto the planet carrier.

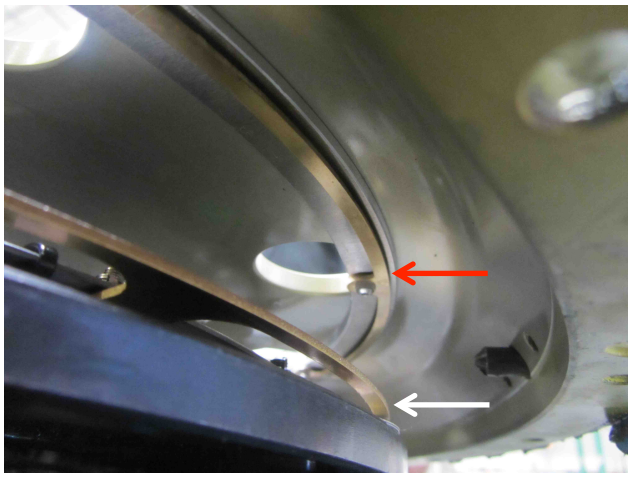


Figure 10. Coils in position before rejoining top cover (static coil red arrow, moving coil white arrow)

Electrical isolation of the coils from the mounts and surrounding metallic structure was achieved through the use of nylon washers and bushes. The main electrical difference between the lab-scale coils and the full-scale coils is their proximity to metal, and in particular, the mounting ring which forms a “shorted turn”. The proximity causes a drastic reduction in inductance, which then requires an increase in loading capacitance to maintain tune at 13.56 MHz. In addition to the reduction in inductance comes a large reduction in the Q factor of the coupled circuit. Fortunately, the electrical power transfer requirement in the gearbox was significantly reduced compared to the prototype, as the spacing between the coils was relatively close. This meant that even with reduced Q, there was enough power transferred to run the opamp buffer circuit. One advantage of reduced Q factor is that dispersion is reduced in the baseband signal. This is because the steepness of the phase/frequency response is reduced in the vicinity of the resonance at 13.56 MHz.

Once installed in the gearbox, it was possible to temporarily attach a signal generator to the sensor boards. By comparing the input signal with the output signal of the system transmitted through the coils, the time delay of the system was measured. From 100 kHz to 1 MHz, there was very little delay variation with frequency - the system is behaving as a length of cable - providing about 1 µs delay at all frequencies. This means that in this range it is linear phase and non-dispersive i.e. there is no variation in wave speed with frequency. Below 100 kHz there is significant dispersion, but since most ‘low’ frequency analysis techniques ignore phase, this is not a significant limitation.

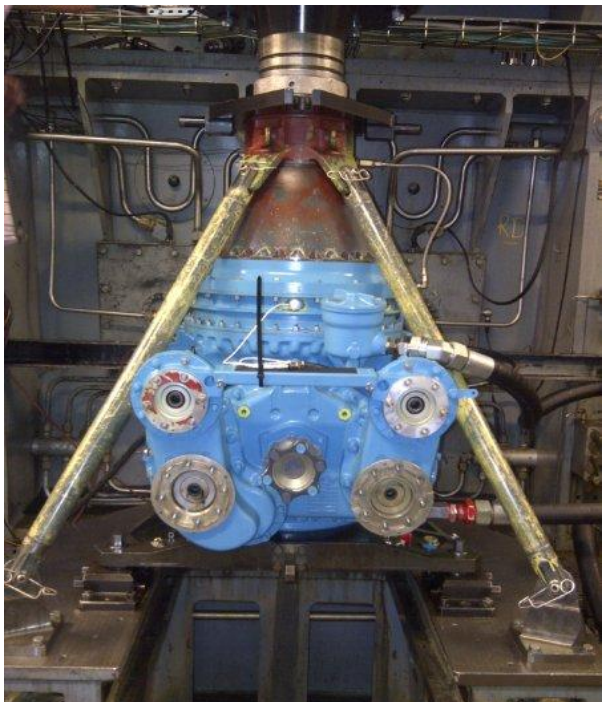


Figure 11. MGB installed on the test bench

In order to replicate a typical HUMS setup, accelerometers were attached to the case of the gearbox using a mixture of bonded and bolted attachments.

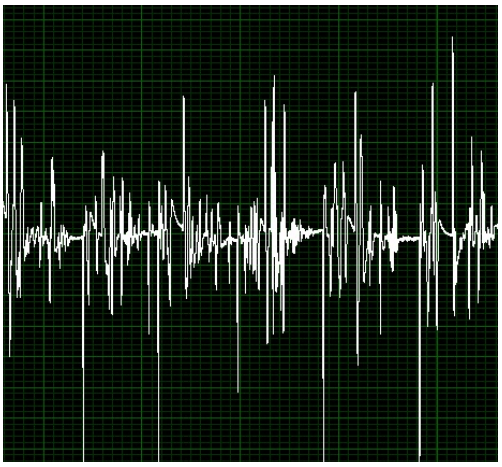


Figure 12. Typical signal from PWAS over wireless transmission

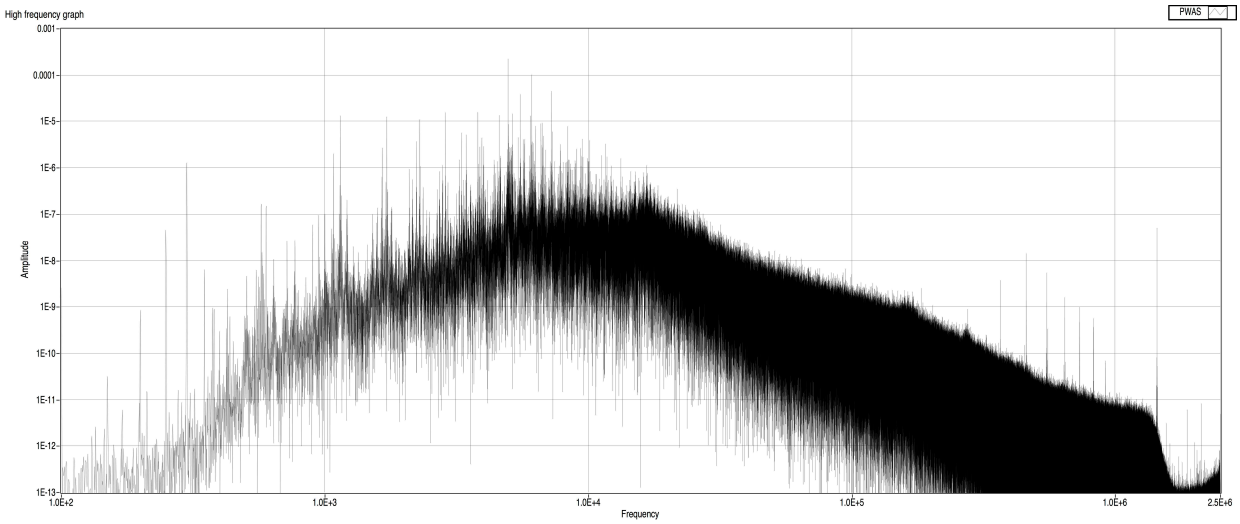


Figure 13. Frequency spectrum of PWAS signal

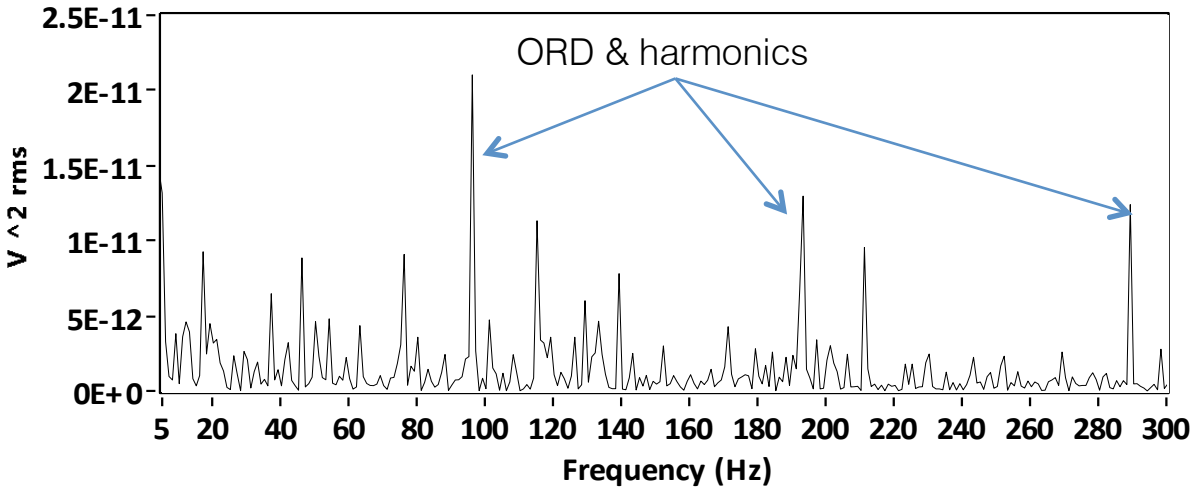


Figure 14. Power spectrum for enveloped random signal for minor damage

8.3.Preliminary Results

The rig was run at power settings ranging from 80% of maximum continuous power (936 kW) to 110% of maximum take-off power (1760 kW) for 20 minutes at each setting. During testing a maximum oil temperature of 97.6 °C was seen.

Figure 12 shows a typical time trace recorded from the PWAS sensor, transmitted wirelessly across the coils. Figure 13 shows the energy content of the corresponding frequency spectrum (including the high pass filter of the sensor conditioning circuit).

The 'low' frequency portion of the signal (of the order of kilohertz) contains clear peaks at typical gear mesh frequencies showing that a meaningful signal is being transferred from the sensor.

Figure 13 shows that the energy levels vary enormously with frequency; typical Fourier amplitudes at 10 kHz are four orders of magnitude larger than those at 1 MHz. It is unusual to be able to make these comparisons since many AE sensors are only useful in a limited frequency range. However, the broadband sensitivity of the PWAS sensor also presents challenges since the large energy levels at low frequency which are present within the gearbox can affect the sensor. It is these high energy levels that are thought to be responsible for the 'dead spots' seen in the time trace as in Figure 12. At high energy levels, the PWAS sensor may saturate and produce no output. This is supported by the repeat frequency of the dead spots which seems to approximately correspond to planet gear mesh frequency. The presence of the dead spots could limit the potential of the signal to provide useful information. However, despite their presence, it was possible to extract useful information from the AE signal.

Figure 14 shows the enveloped random signal for the case of minor damage at 110% maximum take-off power. The outer race defect frequencies and harmonics are clearly visible whereas the undamaged case contained no such harmonics. It can be concluded from this that the sensor is providing useful information across the wireless link at a wide range of frequencies, opening the potential for improved detection.

9. CONCLUDING REMARKS

This research programme has resulted in a successful proof of concept of broadband wireless transmission, including power scavenging, coupled with small-scale broadband sensors, working successfully in an operational environment. This result presents a new range of potential fault diagnosis opportunities for the future of HUMS systems. Future publications will release further results from the testing.

10. ACKNOWLEDGEMENTS

The work described in this paper was conducted as part of EASA.2012.OP.13 VHM. The support of Airbus Helicopters in the full-scale testing is gratefully acknowledged.

11. REFERENCES

[1] Air Accidents Investigation Branch, "Report on the accident to Aerospatiale (Eurocopter) AS332 L2 Super Puma, registration G-REDL 11 nm NE of Peterhead , Scotland on 1 April 2009," EW/C2009/04/01, 2011.

[2] J. T. McKenna, "An Eye on Operations," *Rotor & Wing*, 2005

[3] L. Miller, B. McQuiston, J. Frenster, and D. Wohler, "Rotorcraft Health and Usage Monitoring Systems - A Literature Survey," DOT FAA/RD-91/6, 1991.

[4] J. J. Zakrajsek, P. J. Dempsey, E. M. Huff, M. Augustin, R. Safa-Bakhsh, A. Duke, P. Ephraim, P. Grabil, and H. J. Decker, "Rotorcraft Health Management Issues and Challenges," NASA/TM-2006-214022, 2006.

[5] I. R. Delgado, P. J. Dempsey, and D. L. Simon, "A Survey of Current Rotorcraft Propulsion Health Monitoring Technologies," NASA/TM-2012-217420, 2012.

[6] R. Romero, H. Summers, and J. Cronkhite, "Feasibility Study of a Rotorcraft Health Usage Monitoring System (HUMS): Results of Operator's Evaluation," NASA CR-198446 DOT/FAA/AR-95/50 ARL-CR-289, 1996.

[7] P. J. Dempsey, D. G. Lewicki, and D. D. Le, "Investigation of Current Methods to Identify Helicopter Gear Health," NASA/TM-2007-214664, 2007.

[8] Civil Aviation Authority, "HUMS Extension to Rotor Health Monitoring," CAA Paper 2008/05, 2008.

[9] Chin, K. Danai, and D. G. Lewicki, "Pattern Classifier for Health Monitoring of Helicopter Gearboxes," NASA TM-106099 AVSCOM TR-92-C-033, 1993.

[10] H. Chin, K. Danai, and D. G. Lewicki, "Fault Detection of Helicopter Gearboxes Using the Multi-Valued Influence Matrix Method," NASA TM-106100 AVSCOM TR-92-C-015, 1993.

[11] J. Rafiee, F. Arvani, A. Harifi, and M. H. Sadeghi, "Intelligent condition monitoring of a gearbox using artificial neural network," *Mechanical Systems and Signal Processing*, vol. 21, no. 4, pp. 1746–1754, May 2007.

[12] G. Niu, B.-S. Yang, and M. Pecht, "Development of an optimized condition-based maintenance system by data fusion and reliability-centered maintenance," *Reliability Engineering & System Safety*, vol. 95, no. 7, pp. 786–796, Jul. 2010.

[13] G. Niu and B.-S. Yang, "Intelligent condition monitoring and prognostics system based on data-fusion strategy," *Expert Systems with Applications*, vol. 37, no. 12, pp. 8831–8840, Dec. 2010.

[14] N. S. Swansson, “Application of Vibration Signal Analysis Techniques to Signal Monitoring,” in *Conference on Friction and Wear in Engineering*, 1980, pp. 262–267.

[15] R. M. Stewart, “Some Useful Data Analysis Techniques for Gearbox Diagnostics,” Report MHM/R/10/77, 1977.

[16] S. C. Favaloro, “A Preliminary Evaluation of Some Gear Diagnostics Using Vibration Analysis,” ARL-AERO-RPOP-TM-427, 1985.

[17] H. R. Martin, “Statistical Moment Analysis As a Means of Surface Damage Detection,” in *Proceedings of the 7th International Modal Analysis Conference*, 1989, pp. 1016–1021.

[18] J. J. Zakrajsek, D. P. Townsend, and H. J. Decker, “An Analysis of Gear Fault Detection Methods as Applied to Pitting Fatigue Failure Data,” NASA TM-105950 AVSCOM TR-92-C-035, 1993.

[19] H. J. Decker, R. F. Handschuh, and J. J. Zakrajsek, “An Enhancement to the NA4 Gear Vibration Diagnostic Parameter,” NASA TM-106553 ARL-TR-389, 1994.

[20] J. J. Zakrajsek, R. F. Handschuh, and H. J. Decker, “Application of Fault Detection Techniques to Spiral Bevel Gear Fatigue Data,” NASA TM-106467 ARL-TR-345, 1994.

[21] P. D. Samuel and D. J. Pines, “Constrained adaptive lifting and the CAL4 metric for helicopter transmission diagnostics,” *Journal of Sound and Vibration*, vol. 319, no. 1–2, pp. 698–718, Jan. 2009.

[22] V. V Polyshchuk, F. K. Choy, and M. J. Braun, “Gear Fault Detection with Time-Frequency Based Parameter NP4,” *International Journal of Rotating Machinery*, vol. 8, no. 1, pp. 57–70, 2002.

[23] Civil Aviation Authority, “Intelligent Management of Helicopter Vibration Health Monitoring Report,” CAA Paper 2011/01, 2011.

[24] R. A. Roberts, R. B. Stone, and I. Y. Turner, “Deriving Function-Failure Similarity Information For Failure-Free Rotorcraft Component Design,” in *ASME 2002 Design Engineering technical Conference and Computer and Information In Engineering Conference*, 2002.

[25] H Huang, D Paramo and S Deshmukh, “Unpowered wireless transmission of ultrasound signals“ Smart Mater. Struct. 20, 2011

[26] Randall, R. B. (2004), "Detection and diagnosis of incipient bearing failure in helicopter gearboxes", *Engineering Failure Analysis,* vol. 11, no. 2, pp. 177-190.

[27] Randall, R. B., Sawalhi, N. and Coats, M. (2011), "A comparison of methods for separation of deterministic and random signals", *The International Journal of Condition Monitoring,* vol. 1, no. 1, pp. 11.

[28] Antoni, J. and Randall, R. B. (2001), "optimisation of SANC for Separating gear and bearing signals", *Condition monitoring and diagnostics engineering management,* , no. 1, pp. 89-99.

[29] Ho, D. and Randall, R. B. (2000), "Optimisation of bearing diagnostic techniques using simulated and actual bearing fault signal", *Mechanical Systems and Signal Processing,* vol. 14, no. 5, pp. 763-788.

[30] Antoni, J. (2005), "Blind separation of vibration components: Principles and demonstrations", *Mechanical Systems and Signal Processing,* vol. 19, no. 6, pp. 1166-1180.

[31] Li, Z., Yan, X., Tian, Z., Yuan, C., Peng, Z. and Li, L. (2013), "Blind vibration component separation and nonlinear feature extraction applied to the nonstationary vibration signals for the gearbox multi-fault diagnosis", *Measurement,* vol. 46, no. 1, pp. 259-271.

[32] Barszcz, T. (2009), "Decomposition of vibration signals into deterministic and nondeterministic components and its capabilities of fault detection and identification", *International Journal of Applied Mathematics and Computer Science,* vol. 19, no. 2, pp. 327-335.

[33] Elasha, F., Ruiz-Cárcel, C., Mba, D., Kiat, G., Nze, I. and Yebra, G. (2014), "Pitting detection in worm gearboxes with vibration analysis", *Engineering Failure Analysis,* vol. 42, no. 0, pp. 366-376.

[34] Ruiz-Cárcel, C., Hernani-Ros, E., Cao, Y. and Mba, D. (2014), "Use of Spectral Kurtosis for Improving Signal to Noise Ratio of Acoustic Emission Signal from Defective Bearings", *Journal of Failure Analysis and Prevention,* vol. 14, no. 3, pp. 363-371.

[35] Antoni, J. and Randall, R. (2006), "The spectral kurtosis: application to the vibratory surveillance and diagnostics of rotating machines", *Mechanical Systems and Signal Processing,* vol. 20, no. 2, pp. 308-331.

[36] A. Pickwell, “Design and Development of Micro-electromechanical Acoustic Emission Sensors,” PhD thesis, Cranfield University, 2012.

[37] Giurgiutiu V 2008 *Structural Health Monitoring with Piezoelectric Wafer Active Sensors* (Burlington, MA: Academic)

COPYRIGHT STATEMENT

The author(s) confirm that they, and/or their company or organisation, hold copyright on all of the original material included in this paper. The authors also confirm that they have obtained permission, from the copyright holder of any third party material included in this paper, to publish it as part of their paper. The author(s) confirm that they give permission, or have obtained permission from the copyright holder of this paper, for the publication and distribution of this paper as part of the ERF2014 proceedings or as individual offprints from the proceedings and for inclusion in a freely accessible web-based repository.